



Research Article

## Hydrogen Production via Glycerol Dry Reforming over La-Ni/Al<sub>2</sub>O<sub>3</sub> Catalyst

Kah Weng Siew<sup>1</sup>, Hua Chyn Lee<sup>1</sup>, Jolius Gim bun<sup>1,2</sup>, Chin Kui Cheng<sup>1,2,\*</sup>

<sup>1</sup> Faculty of Chemical & Natural Resources Engineering, Universiti Malaysia Pahang, Lebuhraya Tun Razak, 26300 Gambang, Kuantan Pahang, Malaysia

<sup>2</sup> Center of Excellence for Advanced Research in Fluid Flow, Universiti Malaysia Pahang, Lebuhraya Tun Razak, 26300 Gambang, Kuantan Pahang, Malaysia

Received: 12nd May 2013; Revised: 7th October 2013; Accepted: 16th October 2013

### Abstract

Glycerol (a bio-waste generated from biodiesel production) has been touted as a promising bio-syngas precursor via reforming route. Previous studies have indicated that carbon deposition is the major performance-limiting factor for nickel (Ni) catalyst during glycerol steam reforming. In the current paper, dry (CO<sub>2</sub>)-reforming of glycerol, a new reforming route was carried out over alumina (Al<sub>2</sub>O<sub>3</sub>)-supported non-promoted and lanthanum-promoted Ni catalysts. Both sets of catalysts were synthesized via wet co-impregnation procedure. The physicochemical characterization of the catalyst showed that the promoted catalyst possessed smaller metal crystallite size, hence higher metal dispersion compared to the virgin Ni/Al<sub>2</sub>O<sub>3</sub> catalyst. This was also corroborated by the surface images captured by the FESEM analysis. In addition, BET surface area measurement gave 92.05m<sup>2</sup>/g for non-promoted Ni catalyst whilst promoted catalysts showed an average of 1 to 6% improvement depending on the La loading. Reaction studies at 873 K showed that glycerol dry reforming successfully produced H<sub>2</sub> with glycerol conversion and H<sub>2</sub> yield that peaked at 9.7% and 25% respectively over 2wt% La content. The optimum catalytic performance by 2%La-Ni/Al<sub>2</sub>O<sub>3</sub> can be attributed to the larger BET surface area and smaller crystallite size that ensured accessibility of active catalytic area. © 2013 BCREC UNDIP. All rights reserved

**Keywords:** biofuel; dry reforming; glycerol; hydrogen

**How to Cite:** Siew, K.W., Lee, H.C., Gim bun, J., Cheng, C.K. (2013). Hydrogen Production via Glycerol Dry Reforming over La-Ni/Al<sub>2</sub>O<sub>3</sub> Catalyst. *Bulletin of Chemical Reaction Engineering & Catalysis*, 8 (2): 160-166. (doi:10.9767/bcrec.8.2.4874.160-166)

**Permalink/DOI:** <http://dx.doi.org/10.9767/bcrec.8.2.4874.160-166>

### 1. Introduction

As the world still grappled with energy crunch scenario, there is no indication of slowing demand for fossil fuels; hence a concerted search for alternatives to petroleum based fuels is clearly needed.

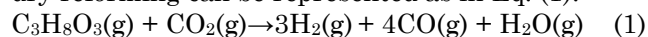
Chief among the identified alternative fuels, hydrogen (H<sub>2</sub>) gas is touted as the most promising option due to its clean emission and high efficiency. Indeed, it has been professed that Malaysia has bright potential in large-scale H<sub>2</sub> production particularly from biomass such as glycerol. The utilization of waste glycerol (from local biodiesel production) potentially lowers the production cost of biodiesel plants [1]. Significantly, B5 palm oil-biodiesel blend has been used in Malaysia [2]. With

\* Corresponding Author.

E-mail: [chinkui@ump.edu.my](mailto:chinkui@ump.edu.my) (C.K. Cheng),

Tel: +60-9-5492896, Fax: +60-9-5492889

large land bank for oil palm cultivation, it provides sustainable availability of raw material for bio-diesel production and hence plethora glycerol by-product. Recently, concerted scientific efforts have been undertaken to produce H<sub>2</sub> gas via steam reforming route. This process requires H<sub>2</sub>O (steam) whilst releasing CO<sub>2</sub> as a byproduct [3]. The primary drawbacks hence are strongly related to the energy-intensive steam production and the release of greenhouse gas CO<sub>2</sub>. Therefore, the current work employs dry reforming process to replace steam reforming. H<sub>2</sub> production via dry reforming technique is reported as a greener process as it consumes CO<sub>2</sub> while releasing H<sub>2</sub>O as the by-product [4]. The availability of bountiful glycerol as the raw material coupled by the green H<sub>2</sub> production (via dry reforming) is believed to offer a better pathway for glycerol dry reforming reaction. The overall glycerol dry reforming can be represented as in Eq. (1):



## 2. Materials and Methods

A series of 0 to 5 wt% La promoted 20 wt% Ni/Al<sub>2</sub>O<sub>3</sub> catalysts were synthesized via co-wet impregnation method. Nitrate solutions of pre-determined metal loadings of respective precursors were mixed with accurately weighed solid alumina. The obtained slurry was then stirred for 3 h and subsequently oven-dried for 24 h. Finally, the dried solid was calcined at 1023 K for 6 h followed by sieving to 90-140 μm. Catalyst characterization was performed to obtain BET surface area, XRD scanning, FESEM imaging and EDX analysis. For glycerol dry reforming experimental work, pristine glycerine grade was directly injected into a 10-mm diameter fixed-bed reactor system at 873 K via a HPLC pump (LabAlliance Series 1) while CO<sub>2</sub> was individually flowed to the reactor as a reforming agent. For all the runs, the ratios of reactants were controlled at unity. N<sub>2</sub> was applied as a carrier gas. Prior to the experiment, H<sub>2</sub> at 50 ml/min was metered into the reactor for catalyst activation. The amount of hydrogen gas produced was determined using Agilent gas chromatography (GC) with TCD capillary columns, HP-MOLSIV (Model No. Agilent 19095P; 30.0 m × 530 μm × 50.0 μm) and HP-Plot/Q column (Model No. Agilent 19095-Q04; 30.0 m × 530 μm × 40.0 μm) under an oven temperature of 393K. Helium gas was used as a carrier gas.

## 3. Results and Discussion

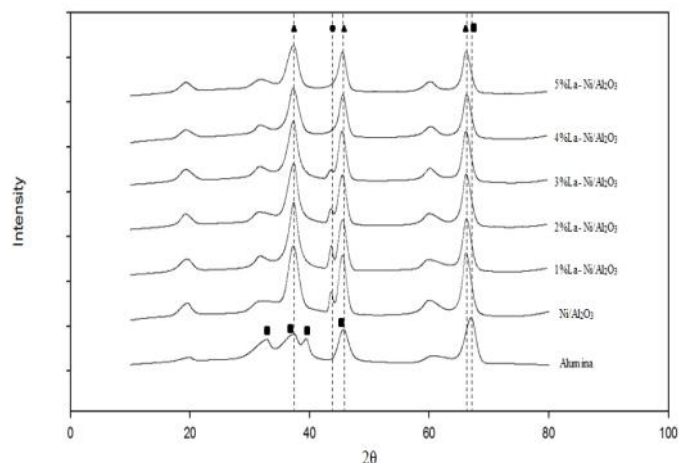
### 3.1. X-Ray Diffraction Characterization

Figure 1 shows the crystallinity structure of calcined catalyst samples via exhibitions of sharp/shoulder peaks at different diffraction angles (2θ).

For pure calcined alumina sample, it can be observed that the XRD pattern only shows the existence of γ-alumina with shorter and broader peaks. This form of alumina support has bigger surface area as proven by the subsequent BET surface area measurements. In addition, it can be observed that the diffraction peak of alumina after impregnation with nickel (resulting in Ni/Al<sub>2</sub>O<sub>3</sub> sample) has shifted to the lower 2θ values. This can be attributed to the diffusion of NiO into the support to form NiAl<sub>2</sub>O<sub>4</sub> phase as confirmed by Zangouei *et al.* [5].

For all the lanthanum (La)-promoted catalysts, it can be seen that similar peaks representing NiAl<sub>2</sub>O<sub>4</sub> phase at 2θ of 37.0°, 44.9° and 65.5° were obtained indicating near-similarity of crystalline structure amongst the samples. Interestingly, La-dopant species was undetectable from the XRD analyses. Most likely, La<sup>3+</sup> which is a considerably large ion and hence difficult to diffuse into the support's vacant sites. Consequently, it exists as La<sub>2</sub>O<sub>3</sub> with high metal dispersion [6] within the solid matrix.

The finely-dispersed La<sub>2</sub>O<sub>3</sub> practically ensures lesser carbon deposition, improves catalyst sintering and an increase in surface area [7]. In addition, the intensities of peaks (including NiO) decreased with La content. Moreover, at 4 wt% and 5 wt%-La respectively, NiO peak was undetectable (cf. Figure 1). The absence of NiO peak indicated that the NiO species was well-dispersed and cannot be detected after a particular level of promoter addition [8]. Furthermore, it seems that the major diffraction peaks had broadened with amounts of La-promoter incorporated indicating formation of smaller crystallites.



**Figure 1:** XRD pattern of prepared calcined catalysts: ■ γ-Al<sub>2</sub>O<sub>3</sub>; ■ NiAl<sub>2</sub>O<sub>4</sub>; ■ NiO

### 3.2 FESEM-EDX Characterization

#### 3.2.1 FESEM Characterization

Figure 2 shows the surface morphology of the catalysts. The particle size and porosity were different for calcined alumina, Ni/Al<sub>2</sub>O<sub>3</sub> and La-Ni/Al<sub>2</sub>O<sub>3</sub> catalysts respectively. For calcined Al<sub>2</sub>O<sub>3</sub> support (cf. Figure 2(a)), it can be observed that the surface was smoother with few crystallites formed and larger pores. This can be supported by the BET surface measurements in Section 3.3 that show surface area of pure calcined alumina as the largest compared to other samples. Post Ni-impregnation, the surface of the Ni/Al<sub>2</sub>O<sub>3</sub> catalyst (cf. Figure 2(b)) becomes rougher. The bulkier and rougher structures were an attribute of both NiO and NiAl<sub>2</sub>O<sub>4</sub> species. The presence of these two species was confirmed by the preceding XRD patterns in Section 3.1. It can also be observed that upon introduction of both Ni and La metals, the pores of the alumina support was blocked by the

formation of new crystallite species, resulting in less porous catalysts.

The FESEM image of 2 wt% La-Ni/Al<sub>2</sub>O<sub>3</sub> catalyst (cf. Figure 2(c)) shows that the crystal particles has smaller crystallite diameter compared to the Ni/Al<sub>2</sub>O<sub>3</sub> due to the ‘spacer’ role played by the La<sub>2</sub>O<sub>3</sub> species that avoids the crystallites from aggregating and forming large particles particles as indicated in Figures 2(c) and 2(d). Consequently, the 2 wt% La-Ni/Al<sub>2</sub>O<sub>3</sub> possesses a higher surface area than the Ni/Al<sub>2</sub>O<sub>3</sub>. Similarly, the FESEM image of 3 wt% La-Ni/Al<sub>2</sub>O<sub>3</sub> (cf. Figure 2(d)) shows even finer crystallite structures or particles compared to 2 wt% La consistent with XRD patterns. Moreover, it can also be observed that the pores on the surface of 3 wt% La-Ni/Al<sub>2</sub>O<sub>3</sub> are nearly unnoticeable as most of the pores had been covered by the smaller crystallite. Hence, an addition of higher promoter amount may not necessarily increase the activity as it may also cover most of the active sites on the catalyst [6].

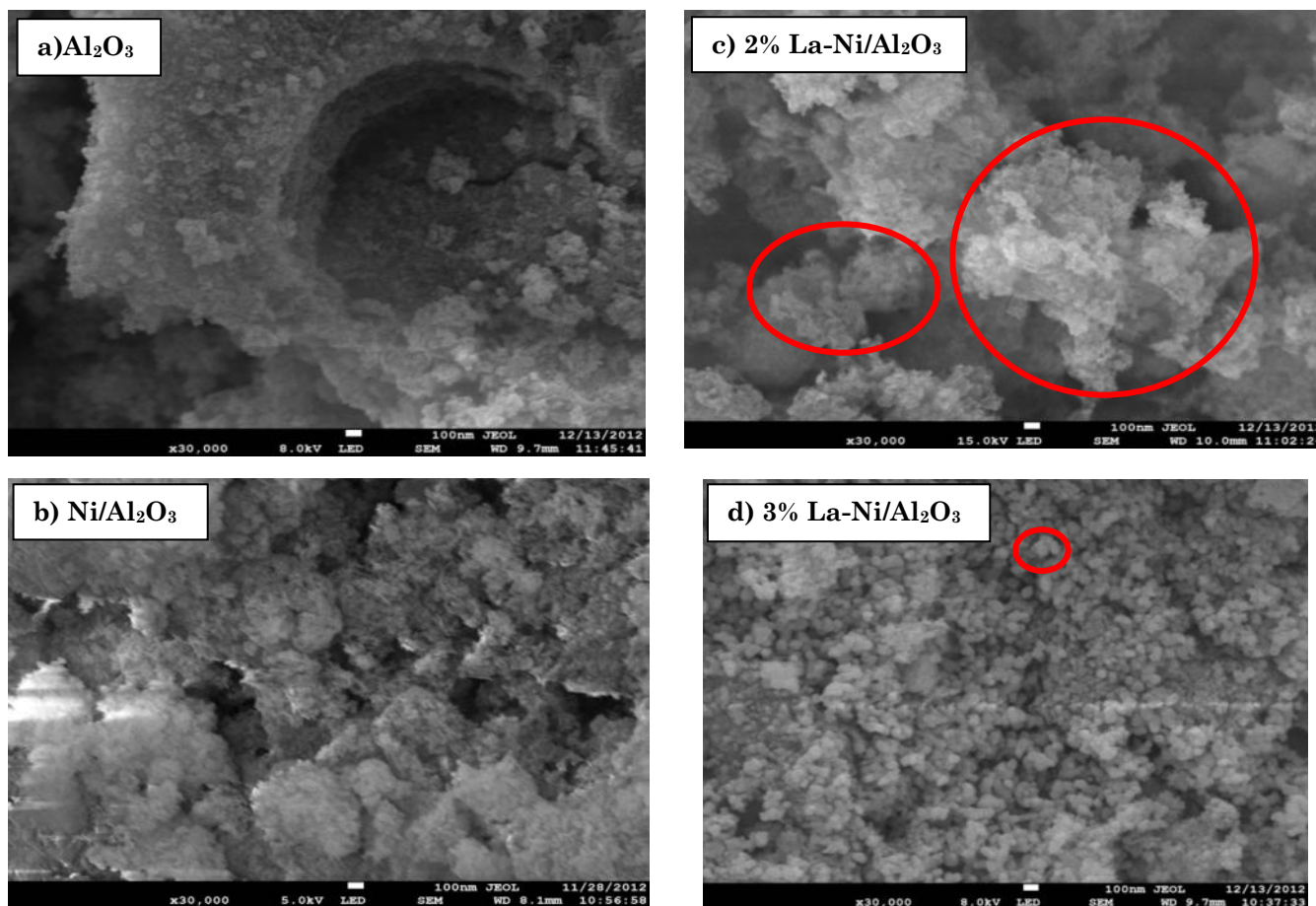


**Figure 2.** Morphology structure of the calcined (a) Al<sub>2</sub>O<sub>3</sub>, (b) Ni-Al<sub>2</sub>O<sub>3</sub>, (c) 2 wt% La-Ni/Al<sub>2</sub>O<sub>3</sub> and (d) 3 wt% La-Ni/Al<sub>2</sub>O<sub>3</sub> catalysts

### 3.2.2 EDX Characterization

EDX measurements were taken to determine the actual metal loading on the synthesized catalysts. Tables 1 to 4 show the actual metal loading detected by EDX analysis for alumina support, unpromoted Ni/Al<sub>2</sub>O<sub>3</sub> catalyst and La-promoted catalyst respectively. Figure 3 illustrates the peaks representing types of element present in unpromoted and several promoted catalysts as function of surface energy (keV). EDX for alumina shows the existence of peaks for Al (1.5 keV), O (at 0.5 keV) and C elements only while EDX pattern for

Ni/Al<sub>2</sub>O<sub>3</sub> records the peaks representing Ni (recorded at 0.9 keV), Al, O and C. The EDX pattern for all La-promoted Ni/Al<sub>2</sub>O<sub>3</sub> catalysts gave peaks for La and Ni elements (superimposed at 1.5 keV), Al, O and C. In addition, the catalyst with higher La promotion (3 wt% La-Ni/Al<sub>2</sub>O<sub>3</sub>) as shown in Figure 3(d) depicts higher La-element peak compared to the lower La promotion catalyst (cf. Figure 3(c)). The existence of C in the result was due to the carbon tape employed to stick the samples onto the sample holder.

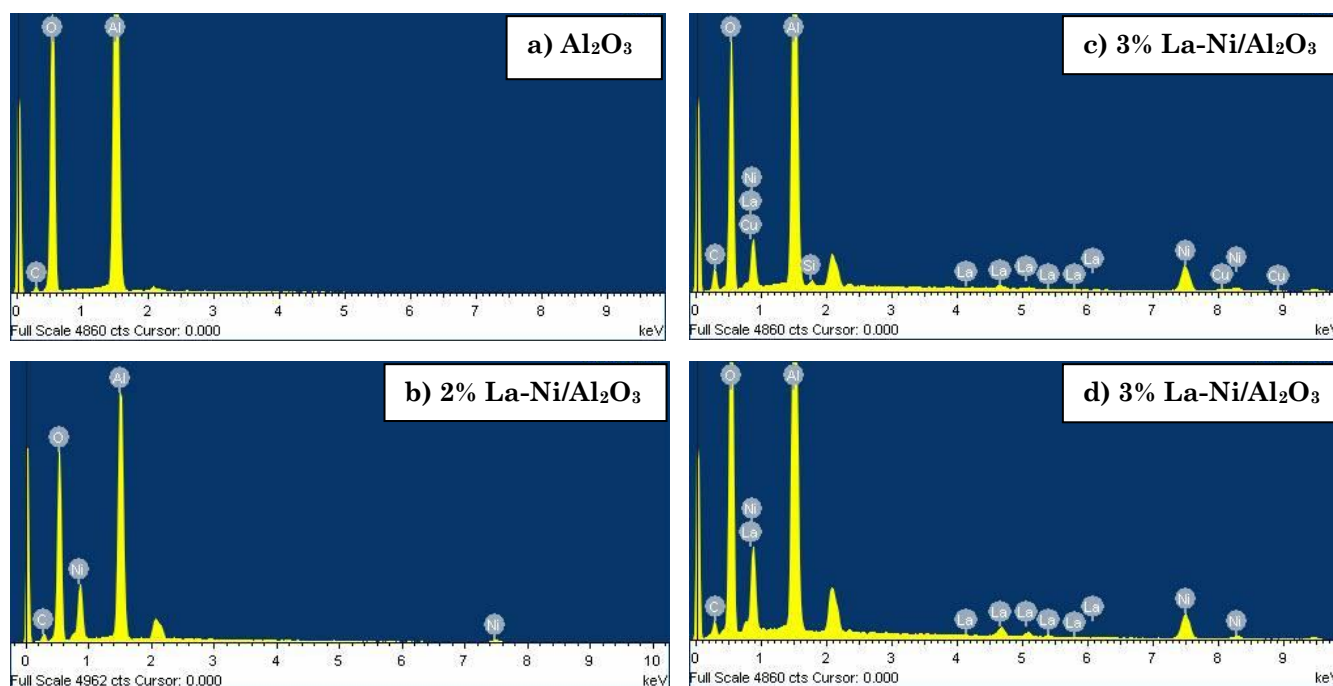


Figure 3. Compositions of elements in the unpromoted and promoted catalysts

Table 1. EDX analysis of alumina

Element	Weight%	Compd%	Formula
C	4.99	18.27	CO <sub>2</sub>
Al	43.26	81.73	Al <sub>2</sub> O <sub>3</sub>
O	51.76		

Table 3. EDX analysis of 2 wt% La-Ni/Al<sub>2</sub>O<sub>3</sub>

Element	Weight%	Compd%	Formula
C	8.12	29.74	CO <sub>2</sub>
Al	25.23	47.66	Al <sub>2</sub> O <sub>3</sub>
Ni	15.75	20.04	NiO
La	1.53	1.80	La <sub>2</sub> O <sub>3</sub>
O	49.02		

Table 2. EDX analysis of Ni/Al<sub>2</sub>O<sub>3</sub>

Element	Weight%	Compd%	Formula
C	4.13	15.12	CO <sub>2</sub>
Al	30.49	57.61	Al <sub>2</sub> O <sub>3</sub>
Ni	21.43	27.27	NiO
O	43.95		

Table 4. EDX analysis of 3 wt% La-Ni/Al<sub>2</sub>O<sub>3</sub>

Element	Weight%	Compd%	Formula
C	4.03	14.77	CO <sub>2</sub>
Al	31.65	59.80	Al <sub>2</sub> O <sub>3</sub>
Ni	17.42	22.16	NiO
La	2.78	3.26	La <sub>2</sub> O <sub>3</sub>
O	44.12		

### 3.3 BET Characterization

The liquid N<sub>2</sub>-isotherms in Figure 4 show similar hysteresis indicative of mesoporous structure for all the synthesized catalysts. Significantly, formation of the type H3 hysteresis loop from the analyses is symptomatic of the aggregation of plate-like material that leads to the formation of slit-like pores [9]. In addition, BET results also showed that all the samples exhibited large specific surface area. It can be seen from Figure 5 that the calcined alumina support has the highest specific surface area (136.9 m<sup>2</sup>/g) among the samples.

The surface area of the Ni/Al<sub>2</sub>O<sub>3</sub> decreased compared to the alumina support because the pores on the alumina support were covered by the loaded nickel species crystallites as aforementioned. Nevertheless, the Ni/Al<sub>2</sub>O<sub>3</sub> catalyst still possessed high surface area (85.0 m<sup>2</sup>/g). Significantly, BET surface area of the 1 wt% La-Ni/ Al<sub>2</sub>O<sub>3</sub> and 2 wt% La-Ni/Al<sub>2</sub>O<sub>3</sub> has increased compared to unpromoted Ni/Al<sub>2</sub>O<sub>3</sub>. This indicates that incorporation of La has increased the surface area catalyst, consistent with the preceding XRD and FESEM results.

Smaller nickel species crystallite has led to a higher surface area. Nonetheless, the surface area of catalysts reduced beyond 2 wt% La loading. Once again, this can be attributed to the more extensive blocking of pores as crystal becomes smaller (cf. Figure 2(d)). Consequently, higher promoter loading may not necessarily enhance the specific surface area.

### 3.4 Reaction Study

Figure 6 shows the result compilation of transient H<sub>2</sub> yields during the dry reforming of glycerol reaction over Al<sub>2</sub>O<sub>3</sub> support, Ni/Al<sub>2</sub>O<sub>3</sub>, and La-promoted Ni/Al<sub>2</sub>O<sub>3</sub> catalysts at 873K for the continuous 120 min. It exhibits the reaction stability and H<sub>2</sub> yield of all reaction runs that rapidly attaining steady-state. At time of 120 min, it can be observed that 2 wt% La-Ni/Al<sub>2</sub>O<sub>3</sub> gave the highest H<sub>2</sub> yield of circa 9.7% while alumina only produced 2%.

It also can be seen that 5 wt% La-doped catalyst showed poorer performance compared to 2 wt% and 3 wt% La-promoted catalysts. As afore-

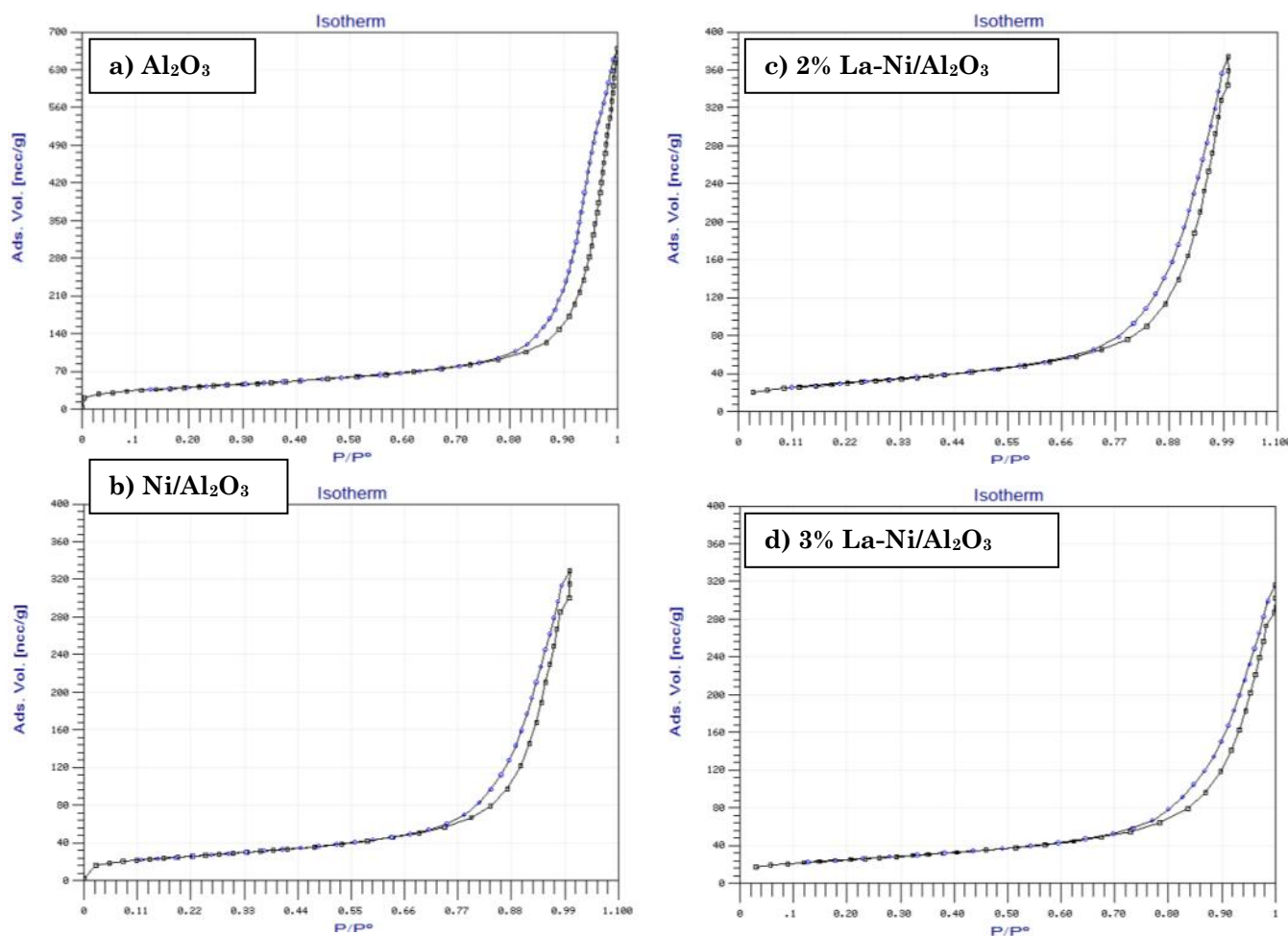


Figure 4. BET isotherm of some catalysts samples

mentioned, this may be explained by the excessive doping of La that resulted in the encapsulation of the available active sites.

Figure 7 shows the H<sub>2</sub> production as a function of La-promotion whilst Figure 8 shows the glycerol conversion trend. Interestingly, both H<sub>2</sub> yield and glycerol conversion exhibited a volcano-shaped curve with respect to the La-metal loading. The H<sub>2</sub> yield and glycerol conversion decreased in the order of 2 wt% La-Ni/Al<sub>2</sub>O<sub>3</sub> > 3 wt% La-Ni/Al<sub>2</sub>O<sub>3</sub> > 4 wt% La-Ni/Al<sub>2</sub>O<sub>3</sub> > 1 wt% La-Ni/Al<sub>2</sub>O<sub>3</sub> > Ni/Al<sub>2</sub>O<sub>3</sub> > 5 wt% La-Ni/Al<sub>2</sub>O<sub>3</sub> > Al<sub>2</sub>O<sub>3</sub>. In particular, both H<sub>2</sub> yield and glycerol conversion for 2 wt% La-Ni/Al<sub>2</sub>O<sub>3</sub> catalyst gave the highest values at time of 120 min reaction, recorded 9.67% and 24.47%, respectively.

Significantly, this can be attributed to the high specific surface area, active sites distribution, highly dispersed metallic nickel species on the catalyst surface, and well-developed mesoporosity in facilitating internal mass transfer of reactant and product in the dry reforming reaction [6].

Against the backdrop of XRD results, it can be concluded that the H<sub>2</sub> production and glycerol conversion has increased when the Ni crystallite size was decreased via La-metal incorporation. However, the addition of La amount exceeding 2 wt% has led to the reduction in both H<sub>2</sub> yields and glycerol conversion although Ni crystallite size is reduced. This is due to La overloading on the catalyst surface. La overloading causes clogging resulting in most of the active site being covered up, hence decreased the catalytic reactivity. Significantly, it has been reported before that excess La amount could cover the active sites of a catalyst [10].

#### 4. Conclusion

The effects of La-promoted Ni based catalyst have been examined and subsequently glycerol dry reforming were carried out at reactant ratio of unity and temperature of 873 K. Physicochemical characterization of the synthesised catalysts re-

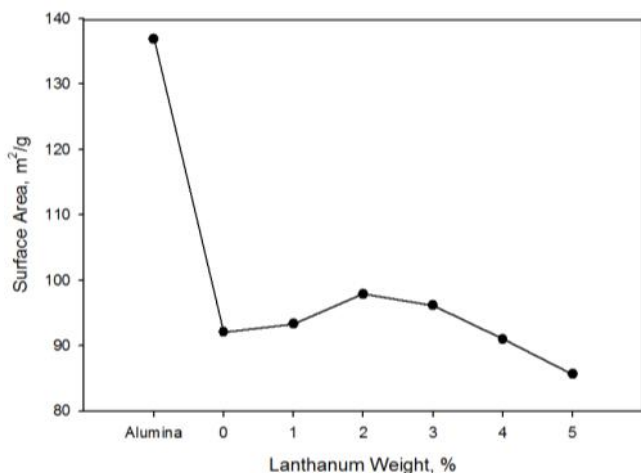


Figure 5. BET Surface area variation at different La loadings

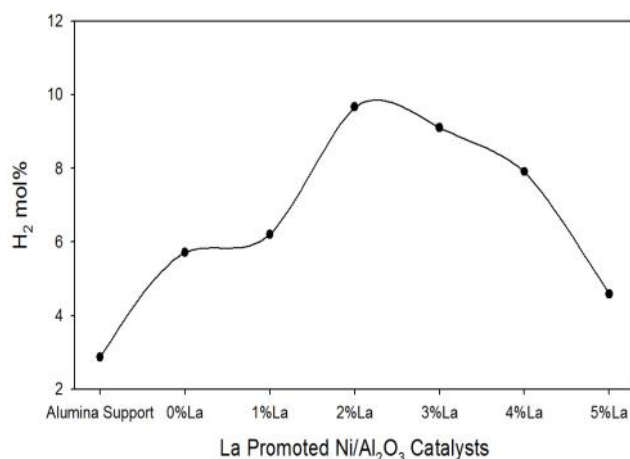


Figure 7. Hydrogen yield as function of La content

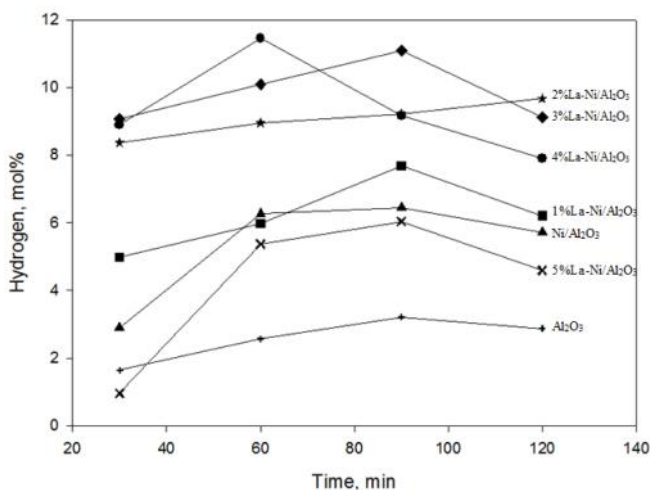


Figure 6. Transient hydrogen yield at 873 K

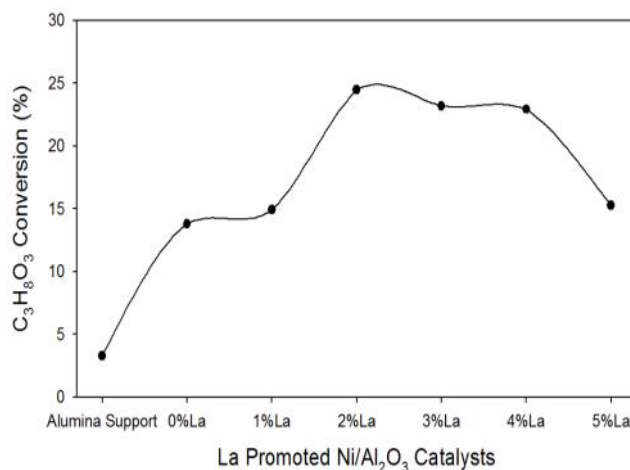


Figure 8. Glycerol conversion as a function of La content

vealed that the addition of La-oxide as promoter has contributed to the fine dispersion of active metal sites over the alumina support. This also explained the larger BET surface area obtained for promoted catalyst compared to the non-promoted Ni/Al<sub>2</sub>O<sub>3</sub> catalyst. Results from glycerol dry reforming experimental works have suggested that this new H<sub>2</sub> producing route is very promising with transient catalytic stability of at least 120 min of reaction and that the best catalytic performance was obtained for reforming over 2 wt% La-Ni/Al<sub>2</sub>O<sub>3</sub> catalyst.

### Acknowledgements

Authors would like to thank MOHE for the provision of MTUN-CoE research grant with vot. no. RDU121216. Kah Weng Siew is a grateful recipient of the GRS scholarship from the Universiti Malaysia Pahang.

### References

- [1] Haas, M.J., McAloon, A.J., Yee, W.C., Foglia, T.A., (2006). A process model to estimate biodiesel production cost., *Bioresour. Technol.* 97(4): 671–678.
- [2] Lim, A., (2011). B5 Biodiesel Programme Begins. Putrajaya Kicks Things Off. Retrieved from <http://paultan.org/2011/06/01/b5-biodiesel-programme-begins-putrajaya-kicks-things-off/>
- [3] O' Sullivan, L. (2008). Hydrogen as an alternative energy source. Environmentalism. Retrieved from <http://suite101.com/article/hydrogen-as-an-alternative-energy-source-a59685#>
- [4] Gao, J., Hou, Z.Y., Lou, H., Zheng, X.M. (2011). Dry (CO<sub>2</sub>) reforming. *Fuel Cells*. 7: 192-213
- [5] Zangouei, M., Zarringhalam, A., Arasteh, M. (2010). The influence of nickel loading on reducibility of NiO/Al<sub>2</sub>O<sub>3</sub> catalysts synthesized by sol-gel method. *Chem. Eng. Research Bulletin* 14: 97-102
- [6] Bang, Y.J., Seo, J.G., Song, I.K. (2011). Hydrogen production by steam reforming of Liquefied Natural Gas (LNG) over mesoporous Ni-La-Al<sub>2</sub>O<sub>3</sub> aerogel catalysts: effect of La content. *Int. J. Hydrogen Energy* 36: 8307-8315
- [7] Lucre' dio, A.F., Jerkiewickz, G., Assaf, E.M. (2007). Nickel catalysts promoted with cerium and lanthanum to reduce carbon formation in partial oxidation of methane reactions. *App. Catal. A: Gen.*, 333: 90–95
- [8] Damyanova, S., Pawele, B., Arishtirova, K., Fierro, J.L.G. (2012). Ni-based catalysts for reforming of methane with CO<sub>2</sub>. *Int. J. Hydrogen Energy*, 37: 15966-15975
- [9] Thommes, M. (2004). Physical adsorption characterization of ordered and amorphous mesoporous materials. *Nanopor. Mat.: Sci. Eng.*, Lu, G.Q., Zhao, X.S. (Eds.), Imperial College Press, Oxford 317
- [10] Natesakhawat, S., Watson, R.B., Wang, X.Q., Ozkan, U.S. (2002). Deactivation characteristics of lanthanide-promoted sol-gel Ni/Al<sub>2</sub>O<sub>3</sub> catalysts in propane steam reforming. *J. Catal.*, 234: 496–508